Computer simulation of ready-to-eat rice reheating on a microwave oven: Application of dielectric mixture equations in foods of varying porosity ratio

Andres ABEA[1], Chihiro SUGIHARA[1], Yvan LLAVE[1*], Saki SUDOU[1], Mark Anthony REDO[1], Maria Dolors GUÀRDIA[2], Israel MUÑOZ[2], Mika FUKUOKA[1],

[1] Department of Food Science and Technology, Tokyo University of Marine Science and Technology, Tokyo, 108-8477, Japan

[2] IRTA, Food Quality and Technology, Monells, 17121, Girona, Catalonia, Spain

* Corresponding author:

Yvan Llave

Department of Food Science and Technology, Tokyo University of Marine Science and Technology, 4-5-7 Konan, Minato-ku, Tokyo, 108-8477, Japan.

E-mail address: pllave1@kaiyodai.ac.jp (Y. Llave)

ABSTRACT

Predictive modeling of dielectric heating in porous foods is challenging due to their nature as multiphase materials. To explore the relationship between the topological structure of multiphase foods and the accuracy of dielectric mixture models, the degree of anisotropy of two cooked rice samples with 26 and 32 % porosity was determined, and their dielectric properties were estimated using the Lichtenecker (LK), Landau-Lifshitz-Looyenga (LLL), and Complex Refractive Index Mixture (CRIM) equations. These properties were used in a predictive finite-element model for reheating an apparent homogeneous rice sample on a flatbed microwave (MW) for 120 s. The results were compared with experimental data and a validated two-element model. Unlike LK and LLL equations, the CRIM equation predicted heat accumulation towards the edges of the container at the two values of porosity ratio evaluated, in accordance with the experimental results and the isotropic nature of the sample. The simulated temperature distributions suggest that the three evaluated equations could predict the MW heating behavior of rice to some extent, but that in order to obtain more accurate results, it could be useful to obtain an empirical topology-related parameter specific for this sample. These results can provide insight on the relationship between the topology of the porous structure in the sample and the adequacy of different dielectric mixture models.

KEYWORDS: Microwave; packed rice; porosity; dielectric mixture equations; anisotropy; computer simulation

1. INTRODUCTION

In recent years, lifestyle changes have led to an increased consumption of ready-to-eat meals, propelling the convenience food industry to surpass the trillion-dollar mark globally (Yadav et al., 2024). Consequently, microwave (MW) heating has been positioned as an indispensable tool, not only for reheating convenience meals in the household but also for their commercial sterilization in the industry (Auksornsri et al., 2018).

When developing ready-to-eat foods or designing industrial thermal treatments, assessing temperature distributions is critical to identifying hot and cold spots and understand their dependence on factors such as formulation or operational parameters (Auksornsri et al., 2018). This is often challenging and resource-intensive, especially when relying on trial-and-error approaches. In this context, computer simulation offers an advanced solution for analyzing heating behavior in domains that are difficult to study experimentally (Zhang et al., 2024).

Rice is a common ingredient in ready-to-eat foods (Auksornsri et al., 2018). It consists of a porous matrix with air and rice phases of varying volume fractions. Simulating MW heating of such foods presents unique challenges due to varying dielectric properties among different phases (Sawale et al., 2024). Although there are methods to measure the dielectric properties of heterogeneous materials, each has its own limitations. For instance, the resonant cavity method is commonly applied but its accuracy is limited to low-loss materials such as oils and plastics (Zhou et al., 2024).

One way to address this challenge is to use dielectric mixture equations. A common form of these models is presented in its general form in Eq. 1, for a mixture of N phases.

$$\varepsilon = \left(\sum_{i=1}^{N} V_i \varepsilon_i^{\alpha} \right)^{\frac{1}{\alpha}} \quad (1),$$

where ε represents the complex dielectric permittivity ($\varepsilon = \varepsilon' - j\varepsilon''$) of the mixture $(-)$, V_i and ε_i are the volume fraction $(-)$ and complex permittivity $(-)$ of each of the phases, respectively, and α is a topology-dependent parameter $(-)$ which ranges between 1 and -1.

The values of $\alpha = -1$ and $\alpha = 1$ in Eq. 1 are known as the Wiener bounds and describe situations of anisotropy where all layers or pores are perpendicular or parallel to an applied external electric field, respectively (Zakri et al., 1998). Between these bounds, for mixtures with a certain level of isotropy in their pore structure, different values of α have been arrived at from different theoretical approaches.

Assuming $\alpha = 0$ for a mixture of two phases a and b, Eq. 2 is obtained:

$$ln\varepsilon = V_a ln\varepsilon_a + V_b ln\varepsilon_b \quad (2).$$

This is often referred to as Lichtenecker's (LK) equation, it was obtained from a semi-empirical basis by Lichtenecker & Rother (1931). Nonetheless it has been applied over the years in multiphase materials and theoretical evidence for it has been provided in recent times (Goncharenko et al., 2000; Simpkin, 2010; Zakri et al., 1998) .

Eq. 3 is obtained by assuming $\alpha = 0.5$:

$$\sqrt{\varepsilon} = V_a\sqrt{\varepsilon_a} + V_b\sqrt{\varepsilon_b} \quad (3).$$

This is commonly called the Complex Refractive Index Mixture (CRIM) equation (Birchak et al., 1974), and it has been arrived at by a number of researchers considering wave propagation through a heterogeneous dielectric mixture. It has a proper theoretical basis when considering the relationship between the complex permittivity of a medium, and the real part of the refractive index of a single electromagnetic wave, which determines the propagation velocity (Birchak et al., 1974; Kraszewski, 1977; Whalley, 1993).

Other values of α have been derived, such as $\alpha = 0.33$ in the case of the Landau-Lifshitz-Looyenga (LLL) equation (Looyenga, 1965):

$$\sqrt[3]{\varepsilon} = V_a \sqrt[3]{\varepsilon_a} + V_b \sqrt[3]{\varepsilon_b} \quad (4).$$

This equation, often cited as assuming a spherical topology, is well known for its versatility and accuracy specially at high frequencies (Khan et al., 1986; Nelson & You, 1990; Nelson, 2000).

Literature dealing with the use of dielectric mixture equations on food products is relatively scarce. Nelson (2005) used different equations to explore the relation between the permittivity of granulated wheat and flour samples and their bulk density, (Liu et al., 2009) used them to obtain the dielectric properties of porous bread considering it a mixture of compact bread and air. Alfaifi et al. (2014) compared different equations in terms of the accuracy to estimate the dielectric properties of a raisins-air two-phase porous system. More recently, they were used by Chen et al. (2019) to simulate radiofrequency heating of a mixture of egg white powder and air, by Yan et al. (2023) to simulate MW heating of a surimi, air, and water mixture, and by Zhang et al. (2024) to estimate the dielectric properties of crushed ice. However, the simulation accuracy at more than one volume fraction was not investigated.

In our previous study (Taguchi et al., 2025), a simulation model for MW heating of cooked rice was developed and validated. However, this model involves dividing the sample domain into rice or air elements, each with distinct physical properties. This can be time-consuming and impractical for certain multiphase foods. Therefore, the aim of the present study is to use this validated model to study the applicability of various mixture equations for estimating the dielectric properties of an apparent homogeneous cooked rice sample. This can provide insight on different ways of accurately predicting the behavior of porous foods during dielectric heating in more effective manner. The specific objectives are:

- To develop MW heating simulation models of cooked rice using an apparent homogenous food approach with different dielectric mixture equations and porosity ratios.

- To compare the temperature distributions predicted with various dielectric mixture equations at two different porosity ratios.
- To explore the relationship between the topological structure of the samples and the accuracy of different dielectric mixture equations at varying porosity ratios.

2. MATERIALS AND METHODS

2.1 Sample preparation

To ensure the homogeneity of the samples used in the experiments, cooked commercial packed rice (Var. Koshihikari, TopValu, Japan) was used. For the heating experiments, the rectangular polypropylene (PP) containers in which the samples are commercially sold were used, since these containers are typically used by consumers to heat the samples at home. To quickly obtain thermal images of the sample's cross section after the experiments, the containers were cut in half along their longitudinal axis. The dimensions of the container and the longitudinal sections are shown in Fig. 1. The two parts were stuck together with heat-resistant tape and the containers were filled with different quantities of cooked rice. Finally, a 0.1 mm polyethylene (PE) film was glued to the top using a household iron.

2.2 Heating experiments

In each experiment the same volume of rice was used, obtained by gently mashing 326 g or 300 g until the original level present in the commercial product was reached, to obtain rice with 26 or 32 % porosity, respectively. These values were chosen based on preliminary trials where porous ratios of ready-to-eat rice from different brands and traditionally prepared rice using a rice cooker were measured. The following relationship was used to obtain the quantity of cooked rice corresponding to each porosity (Li et al., 2019):

$$\phi = 1 - \frac{w_r}{\rho_r V_c} \quad (5),$$

where ϕ is the porosity ratio $(-)$, w_r and ρ_r are the weight (kg) and density (kg/m^3) or rice, respectively, and V_c is the total volume of rice in the container (m^3). Photographs of the sample's longitudinal cross-section can be seen in the supplementary data of this article (Fig. S1).

Prior to heating, the samples were kept at a constant temperature of 20 °C for 6 hours, using a thermostatic chamber (DKN602, Yamato Scientific, Japan). Two optic fiber sensors (FS100-2M, Anritsu, Japan) were inserted into the sample through the PP film according to the positions shown in Fig. 2.

Then, the samples were heated at 600 W for 30 s, 60 s, 90 s, and 120 s using a household flatbed MW oven (MRO-CF6, Hitachi, Japan). This type of oven, commonly used in Japanese households, is equipped with a stirring aluminum antenna that distributes the electric field to obtain varying distributions inside the cavity, eliminating the need for a turntable. The frequency was specified as the nominal value of 2450 MHz and the MW oven and its magnetron were totally cooled down with a fan between experiments.

Finally, the heat-resistant tape was removed, and thermal images were taken using a previously calibrated infrared camera (TH7102WV, NEC San-ei Instruments Inc., Japan) supported by the InfReC Analyzer NS9500 Standard software (Nippon Avionics Co Ltd., Japan). Experiments at each heating time were carried out in triplicate.

2.3 Determination of the porosity and degree of anisotropy

The porosity ratio of each sample was then confirmed using an X-ray computed tomography (CT) scanner (Sky scan 1172 microCT, Bruker, Belgium) to obtain X-ray images of the rice samples. A small cylindrical portion of rice (2.5 cm in diameter × 2 cm in height) was carefully taken from the container and placed in a sample holder with a diameter of 4.5 cm in order to avoid disrupting the internal pore

structure and affecting the porosity. The samples were then scanned under an X-ray source of 59 kV and 100 μA, with a stage rotation of 180 ° rotations with 0.4 ° rotation steps. A total of 1200 projections per sample were obtained using a CCD camera with an image pixel size of 13.59 μm.

The image reconstruction was carried out using the NRecon Skyscan (Bruker, Belgium) software. The software produced two-dimensional axial images with a resolution of 2000 x 2000 pixels. The grayscale pixel values for pure black and white were recorded to be 0 and 255, respectively. The porosity ratio and the degree of anisotropy were then calculated using the CTAn software (Bruker, Belgium).

The degree of anisotropy was calculated using the mean intercept length (MIL) method, where vectors are generated from a random point in the sample, then the MIL from that point are obtained by dividing the length of the vector by the number of hits with a rice/pore intersection. Further, a material anisotropy tensor is established by fitting the MILs to an ellipsoid and the degree of anisotropy is obtained as:

$$Degree\ of\ anisotropy = 1 - \frac{E_s}{E_l} \quad (6),$$

where E_s and E_l are the smallest and largest eigenvalues of the material anisotropy tensor (Yu et al., 2021).

2.4 Predictive model

2.4.1 Model geometry

A commercial FEM software, FEMAP (Ver 10.2 Siemens PLM Software Inc., USA) was used to create the 3D geometric model of the flatbed MW oven and the sample identically to the real geometries (Fig. 3) with the exception of the waveguide. The actual oven has a TE10 (height: 35 mm, width: 85 mm) rectangular waveguide, but to reduce the calculation time the coaxial space at the bottom of the cavity was considered an equivalent coaxial waveguide for the simulation using the method described by Liu et al. (2014a). The heat transfer and electromagnetic equations were solved using the Thermo-HT and

178 the Wavejω-EM modules of the commercial software PHOTO-series (Ver. 7.2, PHOTON Co. Ltd.,
179 Japan) respectively.
180 Two different approaches for the sample model were explored. The first approach was to create a two-
181 element domain using a FORTRAN routine to randomly convert a certain number of rice elements in the
182 sample to void elements, according to the porosity ratios obtained in section 2.2. This method was
183 explained in detail in (Taguchi et al., 2025). The second approach was to consider the sample as an
184 apparent homogeneous dielectric mixture. In this case, each element in the sample domain was assigned
185 the physical properties. Both approaches are illustrated in Fig. 4.
186
187 **2.4.2 Governing equations**
188 The electromagnetic field distribution in space and time is calculated using Maxwell's equations, which
189 are shown below in their differential form (Curet et al., 2008):

$$\nabla \cdot \vec{B} = \nabla \cdot \mu \vec{H} = 0 \tag{7}$$

$$\nabla \cdot \vec{D} = \nabla \cdot \varepsilon \vec{E} = \rho_m \tag{8}$$

$$\nabla \cdot \vec{H} = \frac{\partial \vec{D}}{\partial t} + J = \frac{\partial \varepsilon \vec{E}}{\partial t} + \sigma \vec{E} \tag{9}$$

$$\nabla \cdot \vec{E} = -\frac{\partial \vec{B}}{\partial t} = -\frac{\partial \mu \vec{H}}{\partial t} \tag{10},$$

190 where $\vec{B}$ is the magnetic induction (Wb/m^2), $\vec{H}$ is the magnetic field intensity (A/m), $\vec{D}$ is the electric
191 field displacement (C/m^2), $\vec{E}$ is the electric field intensity (V/m), ρ_m is the electric volume charge
192 density (C/m^3), t is the time (s), J is the current flux (A/m^2), ε is the complex permittivity ($\varepsilon = \varepsilon' - j\varepsilon''$) ($-$), and μ is the magnetic permeability (H/m).

194 The conversion of electromagnetic energy to thermal energy Q (W/m^3) is given by Poynting's theorem
195 (Birla et al., 2008; Choi & Konrad, 1991):

$$Q = 2\pi f \varepsilon_0 \varepsilon'' \left|\vec{E}\right|^2 \quad (11),$$

where ε'' is the dielectric loss factor $(-)$, f is the MW frequency (1/s), and ε_0 is the permittivity of vacuum $(8.854 \times 10^{-12}\, J/(V^2\, m))$. The total heat balance in the model is governed by Fourier's equation (Lan et al., 2020):

$$\rho C_p \frac{\partial T}{\partial t} = \nabla(k \nabla T) + Q \quad (12),$$

where C_p is the specific heat $(J/(kg\ K))$, T is the temperature (K), and k is the thermal conductivity $(W/(m\ K))$.

2.4.3 Assumptions

The aforementioned equations were solved under the following assumptions:

- Given that the samples were kept at a constant temperature and the MW oven was cooled down between experiments, the initial temperature within each domain was assumed as uniform.
- Since no thermal expansion or shrinkage of the samples was observed, and it is not expected to notably affect the trend of transport phenomena in the porous media, it was neglected (Shen et al., 2022).
- The samples were assumed to behave non-magnetically so their permeability was set to that of vacuum ($\mu_0 = 4\pi \times 10^{-7}\ H/m$) (Curet et al., 2008).
- The research focus lied on exploring the adequacy of the dielectric mixture models and the topology of the samples, so phase change and moisture loss were not modeled (Ye et al., 2021).
- The frequency was assumed to be the nominal value of 2450 MHz. While it can vary slightly across equipment and change with time, load position, or dielectric properties, this variability was considered negligible (Chan and Reader, 2000).

2.4.4 Initial and boundary conditions

The following boundary conditions were applied for the governing equations in the predictive model:

- Slide interfaces were assigned to the contact surfaces between rotating and stationary parts (Liu et al., 2014a).
- The initial temperature T_i $(°C)$ of all the domains in the model was set to $20\ °C$ in all simulation runs:

$$T = T_i \text{ at } t = 0 \quad (13).$$

- The oven walls were assumed to be thermally insulated:

$$\nabla T = 0 \quad (14).$$

- The oven walls, coaxial waveguide, and antenna surface were set as perfect electrical conductors, since they are metallic materials expected to reflect electromagnetic radiation almost entirely, resulting in zero normal components of the magnetic and electric fields (Llave et al., 2020):

$$H_n = 0\ , E_n = 0 \quad (15).$$

2.5 Solution method

2.5.1 Time stepping for rotation

The rotation speed of the stirring antenna was set to $120\ °/s$. A time step of 6.666 s was used, which corresponds to a rotation update interval of 400 °. This value was chosen to maximize the accuracy of the model by allowing for 9 calculation steps per cycle according to the antenna rotation speed and the duration of the experiments. The same approach was used by Liu et al. (2014a) for the heating of mashed potatoes on a flatbed MW oven. A schematic diagram of the main simulation steps can be found in (Taguchi et al., 2025).

2.5.2 Calculation of absorbed power

At each time step, the heat transfer module distributes a value of absorbed power according to the electric field distribution obtained by the electromagnetics module. The power absorbed by the samples corresponded to 379.5 W, this value was obtained using a variation of the International Electrotechnical Commission method (IEC, 2014) proposed by Pitchai et al. (2012): $2000\ mL$ of distilled water were heated for $120\ s$ at $600\ W$ (nominal power). The final temperature was recorded and the power absorption Q (J) was calculated as follows:

$$\frac{W C_p \Delta \mathrm{T}}{\Delta \mathrm{t}} = Q \quad (16),$$

where W corresponds to the mass of water (kg) and C_p to its specific heat ($4178\ J/(kg\ K)$) (Choi & Okos, 1986). This method has been applied in a number of studies dealing with MW heating of foods (Kako et al., 2022; Liu et al., 2014b; Yan et al., 2023) and assumes a constant value of absorbed power independent of the dielectric properties of the materials.

2.5.3 Mesh size determination

The model consisted exclusively of hexahedral-shaped elements. The appropriate mesh-size h (mm) relative to the MW wavelength λ (mm) and the relative dielectric constant ε' ($-$) was determined from Eq. 17 (Liu et al., 2013). The total number of elements in all domains was 242236.

$$h = \frac{\lambda}{6\sqrt{\varepsilon'}} \quad (17).$$

All modeling calculations were performed on a workstation with an Intel(R) Core (TM) i7-7700 processor (CPU speed: 3.6 GHz) and 8.00 GB RAM. The calculation time was approximately one week for the two-element model and slightly less than that for the apparent homogeneous models. The meshing

for each individual domain of the model geometry can be found in the supplementary data of this article (Fig.S2).

2.6 Determination of thermophysical and dielectric properties

Temperature-independent thermophysical and dielectric properties of air, PP, and ceramic were obtained from the literature (Krevelen & Nijenhuis, 2009; Liu et al., 2014a). These values, along with the physical properties of the sample elements can be found in Table 1.

2.6.1 Thermophysical and dielectric properties for the two-element model

For the rice elements, temperature-dependent values of dielectric constant, loss factor, thermal conductivity, specific heat, and density of were obtained from (Taguchi et al., 2025).

For the pore elements, the physical properties of air were used except for the thermal conductivity. The reason for this was that it was necessary to account for the heat being transferred by water evaporating at the hot spots, moving through the porous structure of the rice sample, and condensing in the cold spots. Therefore, a value of apparent thermal conductivity was obtained using the same method as in our previous study (Taguchi et al., 2025). This value was also used for the narrow space between the sample and the PE lid, as it was considered that heat transfer could occur in a similar manner in this space.

2.6.2 Thermophysical and dielectric properties of the apparent homogeneous sample

The apparent homogeneous model was tested with three different values of the topology-related parameter α, using the LK ($\alpha = 0$), CRIM ($\alpha = 0.5$), and LLL ($\alpha = 0.33$) mixture formulas (Eqs. 2-4). These values have been used in several studies due to their proper theoretical basis, facilitating comparison with the available literature while covering a somewhat wide range of topologies.

279 The value of penetration depth of microwaves at 2450 MHz was calculated according to the following
280 relationship (Tanaka et al., 2005):

$$d_p = \frac{c}{2\pi f \sqrt{2\varepsilon' \left(\sqrt{1 + \left(\frac{\varepsilon''}{\varepsilon'} \right)^2} - 1 \right)}} \quad (18),$$

281 where c corresponds to the speed of light in vacuum ($2.99 \times 10^8\ m/s$). Penetration depth is defined as
282 the distance at which the power decreases to $1/e$ of its initial value at the surface.
283 For the thermal conductivity, the method reported by Kunii & Smith (1960) was used. In this case, the
284 apparent homogeneous sample was considered as a dispersion of void elements in a continuous phase of
285 cooked rice. Therefore, the apparent thermal conductivity of the mixture k $(W/(m\,K))$ at different
286 temperatures was obtained from the following relationship:

$$k = k_c \left[\phi - \frac{1 - \phi}{\eta + (2/3)(k_a/k_b)} \right] \quad (19),$$

287 where k_a and k_b are the thermal conductivity of rice and void elements respectively, as they were used
288 in the two-element model (section 2.6.1), ϕ is the porosity $(-)$, and η is an empirical constant obtained
289 from the k_a/k_b relation $(-)$. The values obtained at different temperatures were fit to a regression
290 equation for each porosity.
291 The density ρ (kg/m^3) and specific heat C_p $(J/kg\,K)$ of the apparent homogeneous sample were
292 obtained from the volume fractions of rice V_a $(-)$ and air V_b $(-)$ within the sample using the following
293 relations:

$$\rho = V_a \rho_a + V_b \rho_b \quad (20),$$

$$C_p = C_{pa} \rho_a + C_{pb} \rho_b \quad (21),$$

294 where ρ_a and C_{pa} are the density and specific of rice, and ρ_b and C_{pb} are the density and specific heat of
295 air, obtained from (Taguchi et al., 2025).

The value or expression for all the thermophysical properties at 26 and 32 % porosity are shown in Table 1.

2.7 Statistical analysis

To test the differences between experimental and simulated results, the value of root mean square error (RMSE) was obtained from the time-temperature data of N time steps during the MW heating treatments:

$$RMSE = \sqrt{\frac{1}{N}\sum_{i=1}^{N}\left[\frac{T_{exp}(i) - T_{sim}(i)}{T_{exp}(i)}\right]^2} \quad (22),$$

where T_{exp} and T_{sim} are the experimental and simulated temperatures (°C), respectively.

3. RESULTS AND DISCUSSION

3.1 Topology of porous rice

The X-ray CT images of the rice samples at 26 and 32 % are shown in Fig. 5. The values obtained for the degree of anisotropy and porosity ratio are shown in Table 2. The results were considered sufficiently accurate to serve as a confirmation of the porosity of the samples and the corresponding volumetric fractions were used in the calculation of the thermophysical properties of the apparent homogeneous sample.

A qualitative evaluation of the images shows highly interconnected pores in the samples, which ensure gas, water, and heat exchange. No evidence of any ordered pattern or preferred orientation of the pores was observed, which was further confirmed by the low degrees of anisotropy obtained for both samples (Dhaliwal & Kumar, 2022). This is relevant because orientation of the lossy phase in the direction of the electric field benefits charge movement, whereas discontinuity of the lossy phase in the direction of the

electric field causes a depolarization field which reduces the electrical flux density (Fujisaki, 2012). The degree to which there is a preferred orientation of each of the phases defines the topology parameter α that best describes the variation of dielectric properties with the volume fraction of the phases (Leao et al., 2015; Nelson, 1992).

Additionally, the predictive model applied for MW heating in this study accounts for the heat transfer due to vapor movement through the porous structure using a scalar value of apparent thermal conductivity. Therefore, it assumes the isotropy of the vapor diffusivity such that the vapor has no preferable flow direction within the sample (Warning et al., 2014).

3.2 Dielectric properties of the samples

Fig. 6 shows the dielectric properties, and the thermal conductivity of the samples as estimated from the volume fractions obtained in 3.1. It can be seen that in the whole temperature range, CRIM estimated the highest values of dielectric properties, followed by LLL and then by the LK model. This is the expected results when decreasing values of α for a given sample (Regalado, 2004).

The calculated values of the dielectric properties decreased with increasing porosity, as more air inclusions result in fewer polarizable molecules (Liu et al., 2009). The dielectric mixture equations quickly account for this change by using a permittivity value of $\varepsilon = 1 + 0j$ for air. The penetration depth of microwaves increased with porosity since it is inversely related to the dielectric loss factor.

It is worth noting that the estimated values differ more between mixture models than between porosities. This is expected because each model assumes a different pore topology and the effect of the pore shape on the permittivity has been found to be on the order of magnitude of the variation in permittivity due to the porosity ratio (Jones & Friedman, 2000). This results in relatively low values of penetration depth estimated by the CRIM equation: roughly around $2 - 3\,cm$. In contrast, LK equation estimated penetration depths of approximately $3 - 4\,cm$.

341 The calculated thermal conductivity of rice decreased with porosity. This is consistent with the literature;
342 according to Ramesh (2000), thermal conductivity decreases with porosity in cooked rice due to
343 entrapped air which is a worse conductor than rice and water. In our case, an apparent value of thermal
344 conductivity was used for the pore fraction, but increasing its volume ratio still decreases the estimated
345 thermal conductivity of the mixture.
346
347 **3.3 MW heating behavior of cooked rice samples**
348 In the heating experiments, rice was placed in its original PP container, commonly used by consumers.
349 The low height of the container allows for fast and homogeneous heating in the flatbed MW oven used
350 in this study. This is because in this type of oven, microwaves enter from the bottom through the
351 waveguide, as seen in Fig. 7. If the container were taller, greater differences in electric field intensity
352 between the hot spots at the bottom and the cold spots at the top could be expected (Taguchi et al., 2025).
353 It is possible to appreciate the differences in electric field distribution between the two modeling
354 approaches. The two-phase model exhibits highly contrasting electric field intensities, even in contiguous
355 elements (Fig. 7a). In contrast, the electric field gradually distributes in discernible patterns within the
356 apparently homogeneous sample (Fig. 7b), as all its elements share the same dielectric properties.
357 The time-temperature histories of the rice samples during MW heating are shown in Fig. 8, with the
358 corresponding RMSE values listed in Table 3. A slightly faster heating of the 32 % porosity samples was
359 observed, especially from the edges. This is evidenced by the concave shape of the time-temperature
360 history curves in that position. In the 26 % porosity samples, the temperature at the edge was around
361 13 °C higher than that at the center by the end of the heating time. Whereas this difference was around
362 25 °C for the 32 % porosity samples.
363 This heating behavior is also evidence by the temperature distributions shown in Fig. 9. As early as $t = 90\ s$, hot spots can be identified at the edges of the 32 % porosity sample, which are not observed in the

365 26 % sample. This is caused by its lower specific heat and thermal conductivity, which seems to have a
366 greater influence than its slightly higher penetration depth and lower loss factor. Similar results were
367 obtained by Yan et al. (2023) when studying the MW heating behavior of moderate-minced surimi with
368 different porosity ratios.
369 As expected, the two-element model gave good results for both porosities, as indicated by the consistently
370 low RMSE values. The small deviations from the experimental values can be attributed to the various
371 assumptions made in the simulation model. For example, water evaporation can affect the moisture
372 content and heating behavior of the samples, and this effect would also be affected by the porosity ratio
373 due to changes in the effective evaporation area (Li et al., 2019). Additionally, the thermal conductivity
374 of samples such as rice depends on its physical structure, especially of water binding to the starch
375 (Ramesh, 2000). The packed rice samples used in this study have already been thermally treated, but
376 some structural changes may still occur in the starch structure during reheating. Jiang et al. (2022) found
377 changes in the morphology of starch granules, in water binding capacity, and in the ordered structure of
378 starch chains after MW reheating of pregelatinized rice starch.
379 Finally, using calorimetric methods for the calculation of power absorption instead of more setting up
380 devices such as directional couplers can lead to deviations from the experimental conditions since the
381 energy absorption depends on the dielectric properties, geometry, and shape of the load (Kubo et al.,
382 2019; Liu et al., 2014a). The calorimetric methods, however, have been repeatedly validated in several
383 experimental settings; therefore, we consider the deviations originating from these assumptions to be
384 within an acceptable margin.
385
386 **3.4 Dielectric mixture equations**
387 Based on the RMSE values, no clear trend can be observed between the mixture models for the different
388 porosities, with values ranging from 0.06 to 0.35. However, as can be seen in the temperature

389 distributions (Fig. 9), the LK equation predicted heat accumulation towards the center of the container
390 regardless of the porosity ratio, suggesting an overestimation of the penetration depth. This did not result
391 in considerable deviations from the experimental time-temperature histories (Fig. 8) at 26 % porosity but
392 highly overestimated the final central temperature of the 32 % porosity sample resulting in a considerable
393 value of RMSE (0.30).
394 The intermediate penetration depth values calculated with the LLL equation predicted heat accumulation
395 in the center at 32 % porosity, but towards the edges at 26 % porosity. Similar to the LK equation, this
396 caused an abrupt jump towards the end of the time-temperature history curve at the center of the 32 %
397 porosity sample. The prediction for the 26 % porosity sample is in accordance with the experimental
398 values, albeit with a slight overestimation of the temperature difference between the edge and the center.
399 In the case of the CRIM equation, the low penetration depths predicted heat accumulation at the edges
400 of the sample regardless of the porosity ratio which is consistent with the experimental results and the
401 two-element model. The RMSE values were relatively stable but a slight overestimation of the heat
402 generation at the edges was observed.
403 For bread with 80 % porosity, Liu et al. (2009) found that the dielectric constant was predicted more
404 accurately by the LK equation but for the loss factor is was the LLL model the one which provided the
405 best estimations. Ozturk et al. (2018) found better results with the LK and the LLL equations on spices
406 with a volume fraction of around 0.40, and their mixtures. The CRIM equation showed better adequacy
407 to predict the dielectric properties of egg white powder with a volume ratio of 0.80 (Chen et al., 2019).
408 It is clear than the adequacy of one model over another depends more on how the dielectric properties
409 vary with volumetric fraction than on the volumetric fraction itself. Nelson (2005) reported a linear
410 dependency of the cube root of the permittivity of cereal grains and other granulated materials with bulk
411 density, which translated into more reliable estimates by the LLL equation. This linearity, in turn,

412 depends on the topology of the particles in the sample, and how it satisfies the assumptions under which
413 its specific α value was derived (Nelson, 1992).
414 Given the different heating patterns obtained for the mixture equations evaluated in this study, it could
415 be presumed that the value of α for the topology of the air pores in the cooked rice samples used in this
416 study lies somewhere outside of the three values applied in the present study, but closer to 0.5. This is
417 similar to the results obtained by (Leao et al., 2015) for average α values in soil samples. According to
418 the authors, these values suggest that the topology of the porous structure was close to isotropic. This is
419 consistent with the low degree of anisotropy obtained by X-ray CT analysis of the rice samples and
420 supports the apparent thermal conductivity approach applied in the MW heating simulations of the
421 present study.
422 Estimating accurate values or expressions for the α parameter using empirical methods that can better
423 represent the specific topology of the porous structure in different foods is desirable, since it allows for
424 dielectric mixture equations applicable to a wide range of porosity ratios. This gains significance given
425 that the two-element model approach is not feasible with many available finite-element software, and it
426 requires the size of the mesh elements to be comparable to that of the phases, which is not realistic when
427 the particle sizes are small, such as in emulsions or other dispersions.
428 In future studies, it may be desirable to compare the estimated and experimental values of dielectric
429 properties of rice and other multiphase food samples, to determine their specific α values. Additionally,
430 comparing the topological information of various porous foods with the permittivity-porosity
431 relationship could help correlate the α value with the degree of anisotropy and other topological data.
432

433 ## 4. CONCLUSIONS

434 In this study, the dielectric properties of an apparent homogenous rice sample were estimated using
435 various dielectric mixture equations, their accuracy was assessed by comparing them with a two-element

MW heating model and experimental results, and the relationship between the adequacy of the models and the topological structure of the sample was explored at two different porosities. The results of the X-ray CT analysis confirmed the isotropic nature of the cooked rice samples. The evaluated mixture models differed in their capacity to predict the heating behavior at the evaluated porosities. The CRIM equation allowed for accurate predictions of the temperature distribution regardless of the porosity ratio, unlike the LE and the LLL equations. Although the estimation of specific values of α that better reflect the topology of the samples might be useful to obtain more accurate simulation models of dielectric heating processes.

Author statement

Andres Abea: Data curation, formal analysis; investigation; methodology; writing – original draft. Chihiro Sugihara: Formal analysis; investigation; methodology. Saki Sudou: Formal analysis; investigation; methodology. Mark Anthony Redo: Methodology; writing – review and editing. Maria Dolors Guàrdia: supervision; writing – review and editing. Israel Muñoz: supervision; writing – review and editing. Yvan Llave: Conceptualization; supervision; writing – review and editing. Mika Fukuoka: Conceptualization; methodology; resources; supervision; writing – review and editing.

Declaration of competing interest

The authors declare that they have no known competing financial interests or personal relationships that could have appeared to influence the work reported in this paper.

References

458 Alfaifi, B., Tang, J., Jiao, Y., Wang, S., Rasco, B., Jiao, S., & Sablani, S. (2014). Radio frequency
459 disinfestation treatments for dried fruit: Model development and validation. *J. Food Eng.*, *120*,
460 268–276. https://doi.org/10.1016/j.jfoodeng.2013.07.015
461 Auksornsri, T., Tang, J., Tang, Z., Lin, H., & Songsermpong, S. (2018). Dielectric properties of rice
462 model food systems relevant to microwave sterilization process. *Innov. Food Sci. Emerg.*
463 *Technol.*, *45*, 98–105. https://doi.org/10.1016/j.ifset.2017.09.002
464 Birchak, J. R., Gardner, C. G., Hipp, J. E., & Victor, J. M. (1974). High dielectric constant microwave
465 probes for sensing soil moisture. *Proceedings of the IEEE*, *62*(1), 93–98.
466 https://doi.org/10.1109/PROC.1974.9388
467 Birla, S. L., Wang, S., Tang, J., & Tiwari, G. (2008). Characterization of radio frequency heating of
468 fresh fruits influenced by dielectric properties. *J. Food Eng.*, *89*(4), 390–398.
469 https://doi.org/10.1016/j.jfoodeng.2008.05.021
470 Chan, T.C.T, & Reader, H.C. (2000). Understanding microwave heating cavities. Artec House, Boston,
471 USA, pp. 78–81.
472 Chen, J., Lau, S. K., Boreddy, S. R., & Subbiah, J. (2019). Modeling of radio frequency heating of egg
473 white powder continuously moving on a conveyor belt. *J. Food Eng.*, *262*, 109–120.
474 https://doi.org/10.1016/j.jfoodeng.2019.05.029
475 Choi, C. T. M., & Konrad, A. (1991). Finite element modeling of the RF heating process. *IEEE Trans.*
476 *Magn.*, *27*(5), 4227–4230. https://doi.org/10.1109/20.105034
477 Choi, Y., & Okos, M. R. (1986). Effects of temperature and composition on the thermal properties of
478 foods. In *Transport phenomena: Food Engineering and Process Applications* (Vol. 1, pp. 93–
479 101). Elsevier Applied Science.

480 Curet, S., Rouaud, O., & Boillereaux, L. (2008). Microwave tempering and heating in a single-mode
481 cavity: Numerical and experimental investigations. *Chem. Eng. Process. Process. Intensif.*,
482 *47*(9–10), 1656–1665. https://doi.org/10.1016/j.cep.2007.09.011
483 Dhaliwal, J. K., & Kumar, S. (2022). 3D-visualization and quantification of soil porous structure using
484 X-ray micro-tomography scanning under native pasture and crop-livestock systems. *Soil and*
485 *Tillage Research*, *218*, 105305. https://doi.org/10.1016/j.still.2021.105305
486 Fujisaki, K. (2012). Shape anisotropy of electromagnetic materials in application of microwave by
487 micro-sized numerical electromagnetic field calculation. ISIJ Int. *52*(3), 350–354.
488 https://doi.org/10.2355/isijinternational.52.350
489 Goncharenko, A. V., Lozovski, V. Z., & Venger, E. F. (2000). Lichtenecker's equation: Applicability
490 and limitations. *Optics Communications*, *174*(1–4), 19–32. https://doi.org/10.1016/S0030-
491 4018(99)00695-1
492 International Electrotechnical Commission (IEC), 2014. Household Microwave Ovens – Methods for
493 measuring performance. International Electrotechnical Commission.
494 Jiang, J., Li, J., Han, W., Yang, Q., Liu, Q., Xiao, H., Lin, Q., & Fang, Y. (2022). Effects of reheating
495 methods on rheological and textural characteristics of rice starch with different gelatinization
496 degrees. *Foods*, *11*(21), 3314. https://doi.org/10.3390/foods11213314
497 Jones, S. B., & Friedman, S. P. (2000). Particle shape effects on the effective permittivity of anisotropic
498 or isotropic media consisting of aligned or randomly oriented ellipsoidal particles. *Water*
499 *Resour. Res.*, *36*(10), 2821–2833. https://doi.org/10.1029/2000WR900198
500 Kako, Y., Llave, Y., Sakai, N., & Fukuoka, M. (2022). Computer simulation of microwave cooking of
501 sweet potato. *J. Food Process Eng.*, e14121. https://doi.org/10.1111/jfpe.14121
502 Khan, K. M., Shamim, A. & Shah, M. (1986). Application of Looyenga's equation at low frequencies.
503 *J. Mater. Sci. Lett.*, 5, 845–846. https://doi.org/10.1007/BF01729246.

504 Kraszewski, A. (1977). Prediction of the Dielectric Properties of Two-Phase Mixtures. *J. Microwave*
505 *Power.*, *12*(3), 216–222. https://doi.org/10.1080/16070658.1977.11689049
506 Kubo, M.T.K., Curet, S., Augusto, P.E.D. & Boillereaux, L. (2019). Multiphysics modeling of
507 microwave processing for enzyme inactivation in fruit juices. *J. Food Eng.*, *263*, 366–379.
508 https://doi.org/10.1016/j.jfoodeng.2019.07.011.
509 Kunii, D., & Smith, J. M. (1960). Heat transfer characteristics of porous rocks. *AIChE J.*, *6*(1), 71–78.
510 https://doi.org/10.1002/aic.690060115
511 Lan, R., Qu, Y., Ramaswamy, H. S., & Wang, S. (2020). Radio frequency reheating behavior in a
512 heterogeneous food: A case study of pizza. *Innov. Food Sci. Emerg. Technol.*, *65*, 102478.
513 https://doi.org/10.1016/j.ifset.2020.102478
514 Leao, T. P., Perfect, E., & Tyner, J. S. (2015). Evaluation of Lichtenecker's mixing model for
515 predicting effective permittivitty of soils at 50 MHz. *Trans.ASABE*, 83–91.
516 https://doi.org/10.13031/trans.58.10720
517 Li, T., Li, C., Li, C., Xu, F., & Fang, Z. (2019). Porosity of flowing rice layer: Experiments and
518 numerical simulation. *Biosyst. Eng.*, *179*, 1–12.
519 https://doi.org/10.1016/j.biosystemseng.2018.12.003
520 Lichtenecker, K., & Rother, K. (1931). Die Herleitung des logarithmischen Mischungs-gesetzes aus
521 allegemeinen prinzipien der stationaren stro-mung. *The Physical Journal*, *32*, 255–260.
522 Liu, S., Fukuoka, M., & Sakai, N. (2013). A finite element model for simulating temperature
523 distributions in rotating food during microwave heating. *J. Food Eng.*, *115*(1), 49–62.
524 https://doi.org/10.1016/j.jfoodeng.2012.09.019
525 Liu, S., Ogiwara, Y., Fukuoka, M., & Sakai, N. (2014a). Investigation and modeling of temperature
526 changes in food heated in a flatbed microwave oven. *J. Food Eng.*, *131*, 142–153.
527 https://doi.org/10.1016/j.jfoodeng.2014.01.028

528 Liu, S., Yu, X., Fukuoka, M., & Sakai, N. (2014b). Modeling of fish boiling under microwave
529 irradiation. *J. Food Eng.*, *140*, 9–18. https://doi.org/10.1016/j.jfoodeng.2014.04.017
530 Liu, Y., Tang, J., & Mao, Z. (2009). Analysis of bread dielectric properties using mixture equations. *J.*
531 *Food Eng.*, *93*(1), 72–79. https://doi.org/10.1016/j.jfoodeng.2008.12.032
532 Llave, Y., Kambayashi, D., Fukuoka, M., & Sakai, N. (2020). Power absorption analysis of two-
533 component materials during microwave thawing and heating: Experimental and computer
534 simulation. *Innov. Food Sci. Emerg. Technol.*, *66*, 102479.
535 https://doi.org/10.1016/j.ifset.2020.102479
536 Looyenga, H. (1965). Dielectric constants of heterogeneous mixtures. *Physica*, *31*(3), 401–406.
537 https://doi.org/10.1016/0031-8914(65)90045-5
538 Nelson, S.O.; You, T.S. (1990). Relationships between microwave permittivities of solid and
539 pulverised plastics. *J. Phys. D: Appl. Phys. 23*, 346–353. https://doi.org/10.1088/0022-
540 3727/23/3/014
541 Nelson, S. O. (1992). Estimation of permittivities of solids from measurements of pulverized or
542 granular materials. *Prog. Electromagn. Res.*, *06*, 231–271.
543 https://doi.org/10.2528/PIER90010800
544 Nelson, S. O. (2000). Measurement and computation of powdered mixture permittivities. *Proceedings*
545 *of the 17th IEEE Instrumentation and Measurement Technology Conference.* Baltimore, USA. *3*,
546 1159–1162. https://doi.org/10.1109/IMTC.2000.848661
547 Nelson, S. O. (2005). Density-permittivity relationships for powdered and granular materials. *IEEE*
548 *Trans. Instrum. Meas., 54*(5)*,* 2033–2040. https://doi.org/10.1109/TIM.2005.853346
549 Ozturk, S., Kong, F., Singh, R. K., Kuzy, J. D., Li, C., & Trabelsi, S. (2018). Dielectric properties,
550 heating rate, and heating uniformity of various seasoning spices and their mixtures with radio
551 frequency heating. *J. Food Eng.*, *228*, 128–141. https://doi.org/10.1016/j.jfoodeng.2018.02.011

552 Ramesh, M. N. (2000). Effect of cooking and drying on the thermal conductivity of rice. *Int. J. Food*
553 *Prop.*, *3*(1), 77–92. https://doi.org/10.1080/10942910009524617
554 Regalado, C. M. (2004). A physical interpretation of logarithmic TDR calibration equations of volcanic
555 soils and their solid fraction permittivity based on Lichtenecker's mixing formulae. *Geoderma*,
556 *123*(1–2), 41–50. https://doi.org/10.1016/j.geoderma.2004.01.026
557 Sawale, M., Benyathiar, P., Coronel, P., Rawat, A., Simunovic, J., Ozadali, F., & Mishra, D. K. (2024).
558 Aseptic microwave sterilization and validation of food containing particles. *Food Bioprod.*
559 *Process.*, *143*, 28–35. https://doi.org/10.1016/j.fbp.2023.10.001
560 Shen, L., Gao, M., Feng, S., Ma, W., Zhang, Y., Liu, C., Liu, C., & Zheng, X. (2022). Analysis of
561 heating uniformity considering microwave transmission in stacked bulk of granular materials on
562 a turntable in microwave ovens. Journal of Food Engineering, 319, 110903.
563 https://doi.org/10.1016/j.jfoodeng.2021.110903
564 Simpkin, R. (2010). Derivation of Lichtenecker's logarithmic mixture formula from Maxwell's
565 equations. *IEEE Trans. Microw. Theory Tech.s*, *58*(3), 545–550.
566 https://doi.org/10.1109/TMTT.2010.2040406
567 Succar, J., & Hayakawa, K. I. (1983). Empirical formulae for predicting thermal physical properties of
568 fod at freezing or defrosting temperatures. *J. Food Sci. Technol.*, *16*(6), 326–331.
569 Sweat, V. (1994). Thermal Properties of Foods. In *Engineering Properties of Foods* (2nd ed., pp. 99–
570 139). Marcel Dekker Inc.
571 Taguchi, Y., Abea, A., Llave, Y., Sugihara, C., Suzuki, F., Hosoda, T., Onizawa, K., Sakai, N.,
572 Fukuoka M. (2025). Modeling of microwave thawing and reheating of multiphase foods: A case
573 study for packed rice. *J. Food Eng.*, 386, 112284.
574 https://doi.org/10.1016/j.jfoodeng.2004.10.023

575 Tanaka, F., Morita, K., Mallikarjunan, P., Hung, Y.C., & Ezeike, G. O. I. (2005). Analysis of dielectric
576 properties of soy sauce. *J. Food Eng.*, *71*(1), 92–97.
577 https://doi.org/10.1016/j.jfoodeng.2004.10.023
578 Warning, A., Verboven, P., Nicolai, B., van Dalen, G., & Datta, A. (2014). Computation of mass
579 transport properties of apple and rice from X-ray microtomography images. *Innov. Food Sci.*
580 *Emerg. Technol., 24*, 14–27. https://10.1016/j.ifset.2013.12.017
581 Whalley, W. R. (1993). Considerations on the use of time-domain reflectometry (TDR) for measuring
582 soil water content. *J. Soil Sci.*, *44*(1), 1–9. https://doi.org/10.1111/j.1365-2389.1993.tb00429.x
583 Yadav, G. P., Kumar, D., Dalbhagat, C. G., & Mishra, H. N. (2024). A comprehensive review on
584 instant rice: Preparation methodology, characterization, and quality attributes. *Food Chem.*
585 *Adv.*, *4*, 100581. https://doi.org/10.1016/j.focha.2023.100581
586 Yan, B., Meng, L., Yang, H., Du, L., Jiao, X., Zhang, N., Huang, J., Zhao, J., Zhang, H., Chen, W., &
587 Fan, D. (2023). Microwave heating process of moderate-minced surimi based on multiphase
588 porous media model. *J. Food Sci.*, *88*(1), 273–292. https://doi.org/10.1111/1750-3841.16408
589 Ye, J., Xu, C., Zhang, C., Zhu, H., Huang, K., Li, Q., Wang, J., Zhou, L., & Wu, Y. (2021). A hybrid
590 ALE/implicit function method for simulating microwave heating with rotating objects of
591 arbitrary shape. Journal of Food Engineering, 302, 110551.
592 https://doi.org/10.1016/j.jfoodeng.2021.110551
593 Yu, Q., Wang, M., Tian, Y., Shi, X., Li, X., Xu, L., Xie, X., Shi, Y., & Zhu, Y. (2021). Effects of
594 porous clay ceramic rates on aeration porosity characteristics in a structurally degraded soil
595 under greenhouse vegetable production. *Pedosphere, 31 (4)*, 606–614. 10.1016/S1002-
596 0160(21)60006-1

Zakri, T., Laurent, J.-P., & Vauclin, M. (1998). Theoretical evidence for `Lichtenecker's mixture formulae' based on the effective medium theory. *J. Phys. D: Appl. Phys.*, *31*(13), 1589–1594. https://doi.org/10.1088/0022-3727/31/13/013

Zhang, Y., Chen, X., Liu, Y., Li, F., Tang, J., Shi, H., & Jiao, Y. (2024). Using ice surrounding to improve radio frequency tempering uniformity of bulk pacific white shrimp (*Litopenaeus vannamei*). *J. Food Eng.*, *371*, 111967. https://doi.org/10.1016/j.jfoodeng.2024.111967

Zhou, X., Czekala, P., Olszewska–Placha, M., Salski, B., Zhang, S., Pedrow, P. D., Sablani, S. S., & Tang, J. (2024). Understanding microwave heating of oils. *J. Food Eng.*, *375*, 112039. https://doi.org/10.1016/j.jfoodeng.2024.112039

Figure captions

Figure 1. Bottom (a), top (b) and lateral view (c) of the polypropylene container three-dimensional model, and longitudinal cut (d) for the inner temperature examination after the rice reheating experiments (all sizes are in millimeters).

Figure 2. Position of the optic fiber sensors at the corner (a) and center (b) of the sample during the heating experiments or rice on a flatbed MW oven (all sizes are in millimeters).

Figure 3. Schematic diagrams of the flatbed microwave oven and sample container used in this study. View from the z-x (a) z-y (b) and x-y (c) directions (all sizes are in millimeters).

Figure 4. The two approaches used in the three-dimensional modeling of the rice samples.

Figure 5. X-ray computed tomography images of the rice samples with 26 % (a) and 32 (b) % porosity for determination of porosity ratio and degree of anisotropy.

618 **Figure 6**. Calculated dielectric constant (a), dielectric loss factor (b), penetration depth (c) and apparent
619 thermal conductivity (d) of the apparent homogeneous sample model obtained with various mixture
620 equations at 26 and 32 % porosity from 20 to 90 °C.

621 **Figure 7**. Frontal cross-section of the electric field distribution (V/m) during MW reheating of cooked
622 rice on a flatbed microwave oven (t=20 s) simulated using a two-element (a) and apparent homogeneous
623 (b) model.

624 **Figure 8**. Experimental (mean values ± standard deviation, *n*=3) and simulated temperatures as function
625 of MW heating time for: 26 % porosity rice at the edge (a), 26 % porosity rice at the center (b), 32 %
626 porosity rice at the edge (c), and 32 % porosity rice at the center (d) of the container.

627 **Figure 9.** Experimental temperature distribution of the longitudinal cross-section (Z-Y view) of 26 and
628 32 % porosity rice samples during heating on a flatbed MW oven and simulated results using different
629 approaches.

630

631

Highlights

- Microwave reheating simulations of an apparent homogeneous rice sample were built.
- Samples at two porosity values were modeled using dielectric mixture equations.
- Cooked rice samples at the evaluated porosity values had low degree of anisotropy.
- Different topologies assumed by each equation result in different heating patterns.
- The complex refractive index mixture equation shows slightly more accurate results.

639 **Table 1.** Physical properties of the materials used in the predictive simulation model of rice reheating

640 on a flatbed microwave model.

Parameter	Value or equation	Source
Dielectric constant $\varepsilon^{'}$ $[-]$		
Rice	$-0.0046T^2 + 0.3218T + 46.535$	Taguchi et al., 2024
Pores	1	Liu et al., 2014a
Air	1	Liu et al., 2014a
Apparent homogeneous sample 26 % (LK)	$-0.0013T^2 + 0.0901T + 17.151$	Present study
Apparent homogeneous sample 32 % (LK)	$-0.0009T^2 + 0.0655T + 13.641$	Present study
Apparent homogeneous sample 26 % (CRIM)	$-0.0027T^2 + 0.1933T + 27.942$	Present study
Apparent homogeneous sample 32 % (CRIM)	$-0.0023T^2 + 0.1659T + 24.395$	Present study
Apparent homogeneous sample 26 % (LLL)	$-0.0023T^2 + 0.1628T + 24.688$	Present study
Apparent homogeneous sample 32 % (LLL)	$-0.0019T^2 + 0.1339T + 20.963$	Present study
Loss factor $\varepsilon^{''}$ $[-]$		
Rice	$0.0015T^2 - 0.2947T + 19.408$	Taguchi et al., 2024
Pores	0	Liu et al., 2014a
Air	0	Liu et al., 2014a
Apparent homogeneous sample 26 % (LK)	$0.0003T^2 - 0.0708T + 4.9123$	Present study
Apparent homogeneous sample 32 % (LK)	$0.0003T^2 - 0.0516T + 3.5642$	Present study
Apparent homogeneous sample 26 % (CRIM)	$0.0007T^2 - 0.1501T + 10.609$	Present study
Apparent homogeneous sample 32 % (CRIM)	$0.0006T^2 - 0.1289T + 9.1008$	Present study
Apparent homogeneous sample 26 % (LLL)	$0.0006T^2 - 0.1266T + 8.9245$	Present study
Apparent homogeneous sample 32 % (LLL)	$0.0005T^2 - 0.1043T + 7.3376$	Present study
Specific heat C_p $[J/kg\ K]$		
Rice	3080	Taguchi et al., 2024
Pores	1200	Liu et al., 2014a
Air	1200	Liu et al., 2014a
Apparent homogeneous sample 26 %	2478.54	Present study
Apparent homogeneous sample 32 %	2416.32	Present study
Density ρ $[kg/m^3]$		
Rice	1060	Taguchi et al., 2024
Pores	1.2	Liu et al., 2014a
Air	1.2	Liu et al., 2014a
Apparent homogeneous sample 26 %	787.70	Present study
Apparent homogeneous sample 32 %	721.17	Present study
Thermal conductivity k $[W/m\ K]$		
Rice	0.319	Succar & Hayakawa, 1983
Pores	$0.025\ exp(0.116(T - 20))$	Taguchi et al., 2024
Air	0.025	Liu et al., 2014a
Apparent homogeneous sample 26 %	$0.023\ exp(0.067T)$	Present study
Apparent homogeneous sample 32 %	$0.035\ exp(0.056T)$	Present study

641 T: Temperature [°C]

642

643

644 **Table 2.** Values of porosity and degree of anisotropy of the two packed rice samples used in the

645 microwave heating experiments.

Sample	Porosity (%)	Degree of anisotropy (-)
26 %	26.34 ± 0.75	0.14 ± 0.01
32 %	32.49 ± 1.09	0.18 ± 0.02

646

647

Table 3. Values of RMSE for the four approaches used in this study to simulate rice samples during heating on a flatbed microwave oven for 120 s.

Model	RMSE edge (-)	RMSE center (-)
Two-element model		
26 %	0.13	0.15
32 %	0.07	0.07
Apparent homogeneous model LK equation		
26 %	0.20	0.07
32 %	0.15	0.30
Apparent homogeneous model CRIM equation		
26 %	0.29	0.09
32 %	0.26	0.06
Apparent homogeneous model LLL equation		
26 %	0.35	0.13
32 %	0.18	0.18

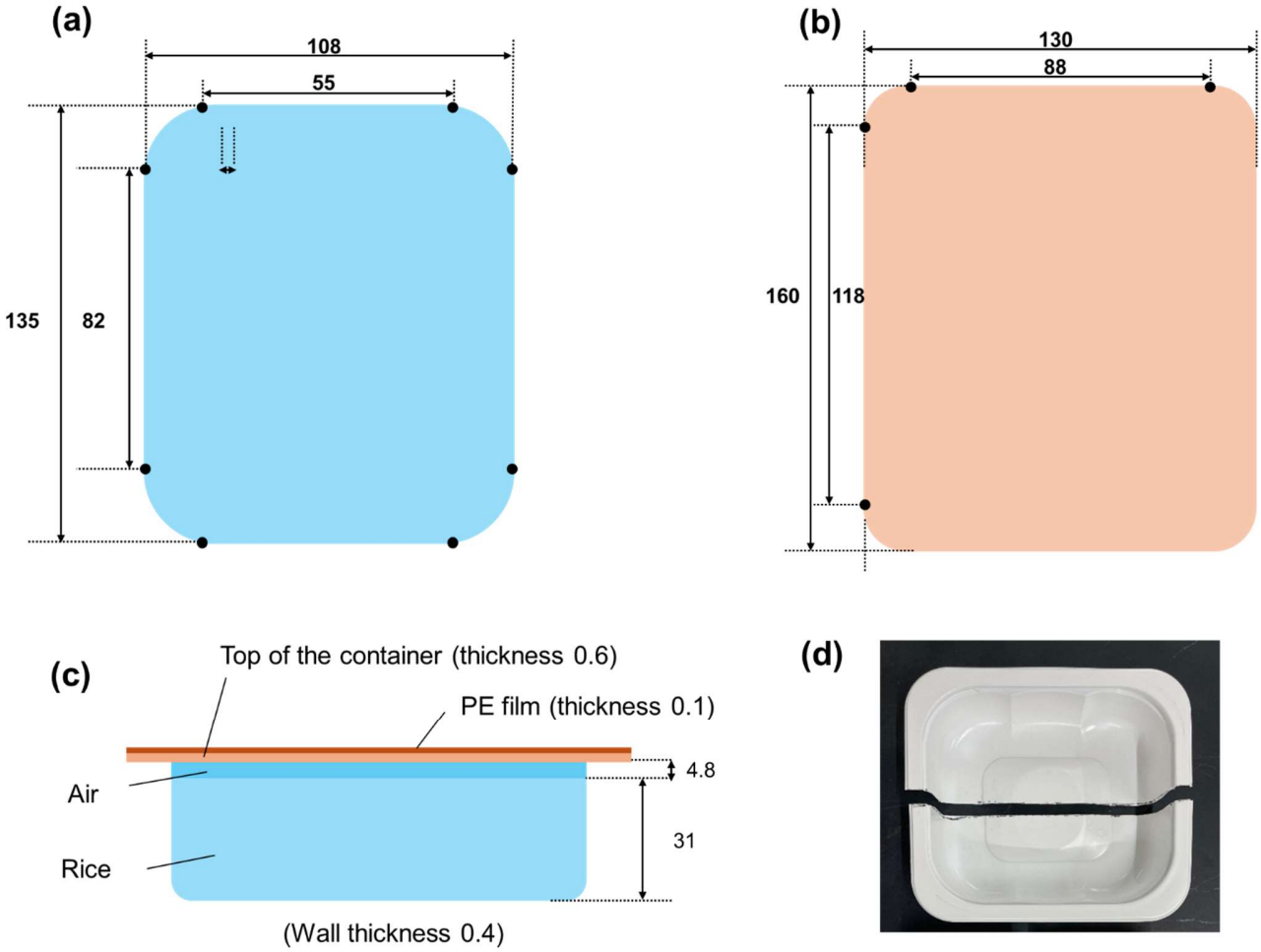

652

653 **Figure 1.** Bottom (a), top (b) and lateral view (c) of the polypropylene container three-dimensional

654 model, and longitudinal cut (d) for the inner temperature examination after the rice reheating

655 experiments (all sizes are in millimeters).

656

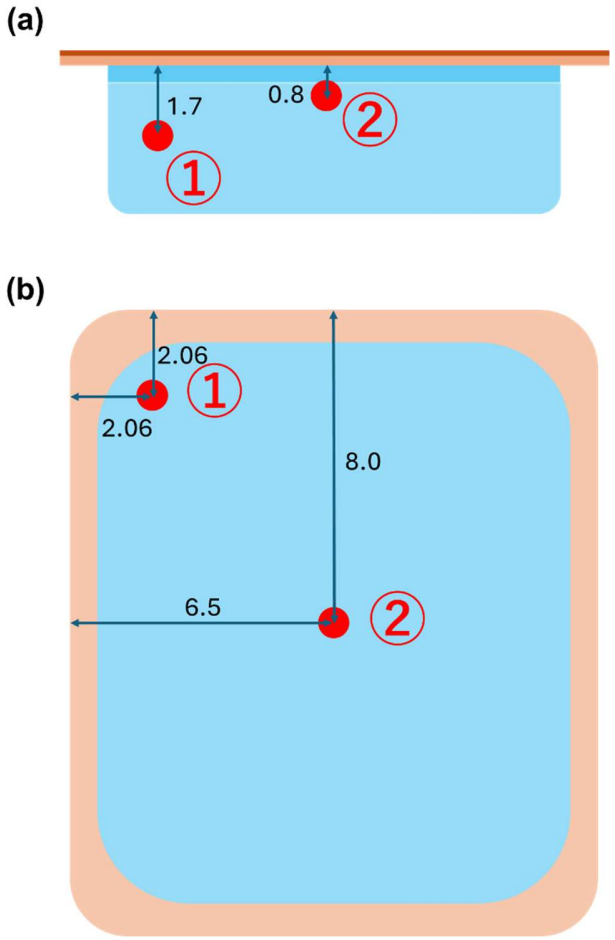

Figure 2. Position of the optic fiber sensors at the corner (a) and center (b) of the sample during the heating experiments or rice on a flatbed MW oven (all sizes are in millimeters).

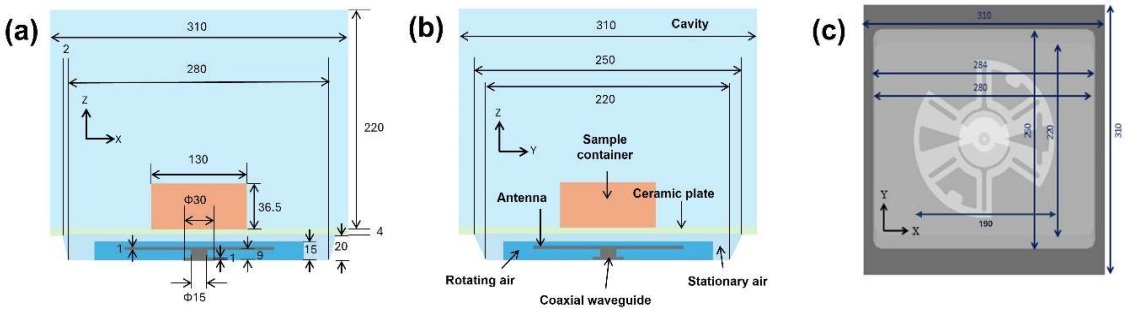

660

661 **Figure 3**. Schematic diagrams of the flatbed microwave oven and sample container used in this study.

662 View from the z-x (a) z-y (b) and x-y (c) directions (all sizes are in millimeters).

663

664

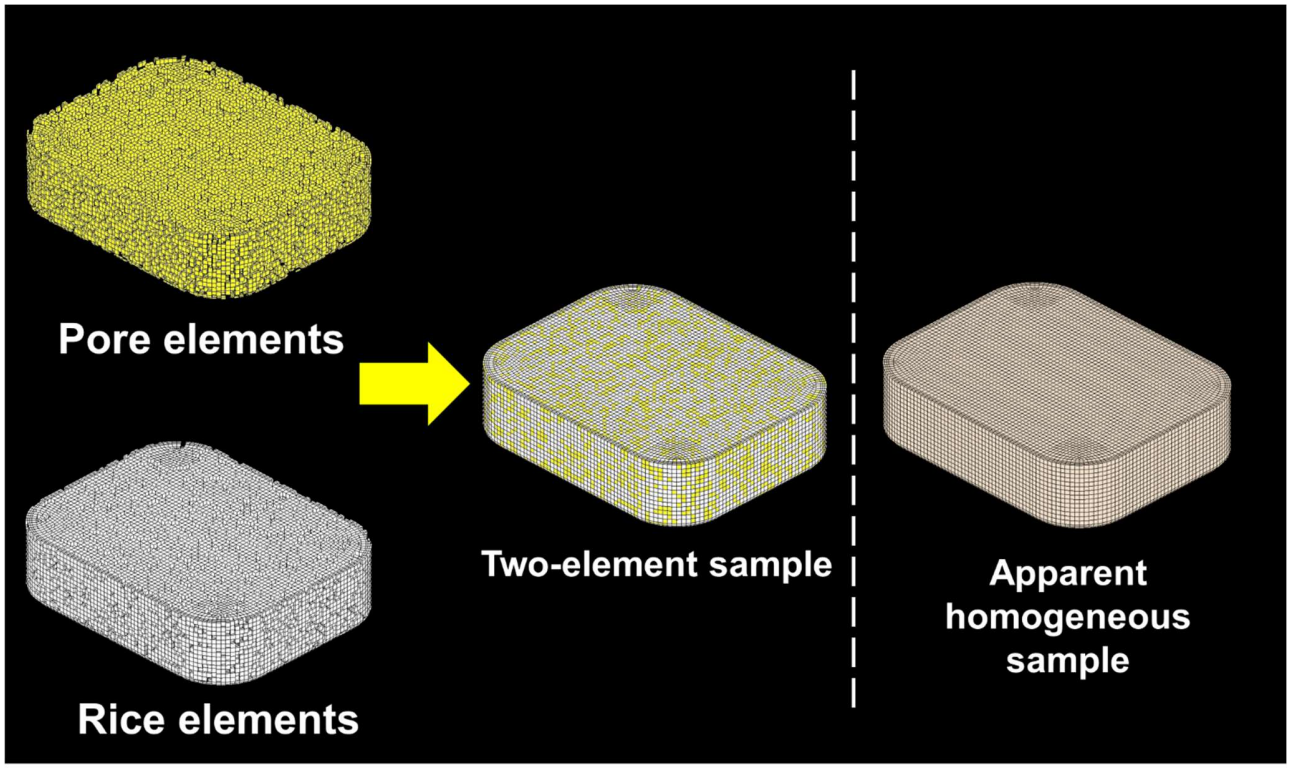

665

666 **Figure 4**. The two approaches used in the three-dimensional modeling of the rice samples.

667

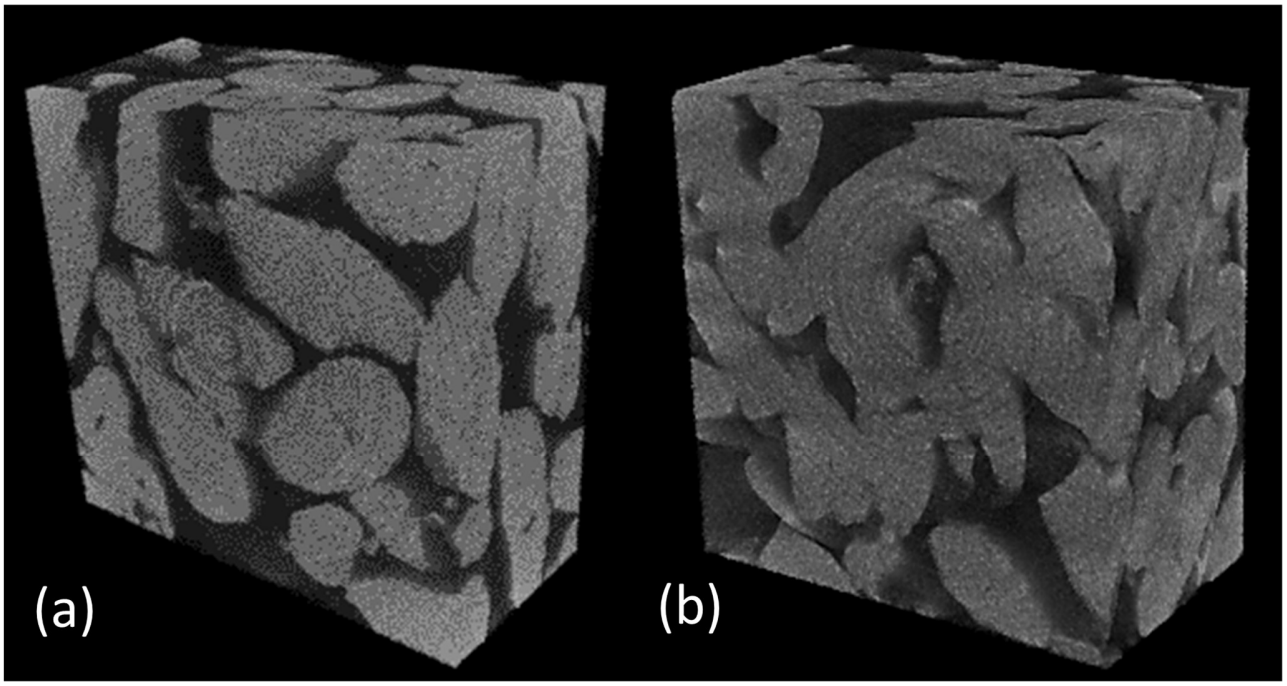

668

669 **Figure 5**. X-ray computed tomography images of the rice samples with 26 % (a) and 32 (b) % porosity

670 for determination of porosity ratio and degree of anisotropy.

671

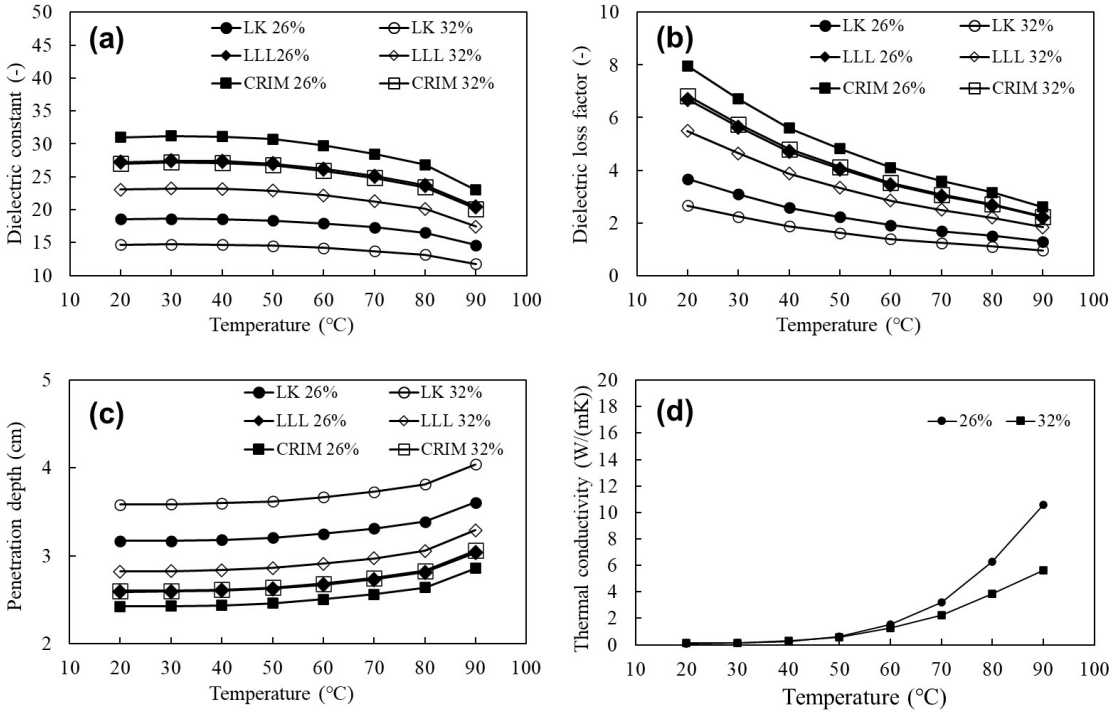

672

673 **Figure 6**. Calculated dielectric constant (a), dielectric loss factor (b), penetration depth (c) and apparent

674 thermal conductivity (d) of the apparent homogeneous sample model obtained with various mixture

675 equations at 26 and 32 % porosity from 20 to 90 °C.

676

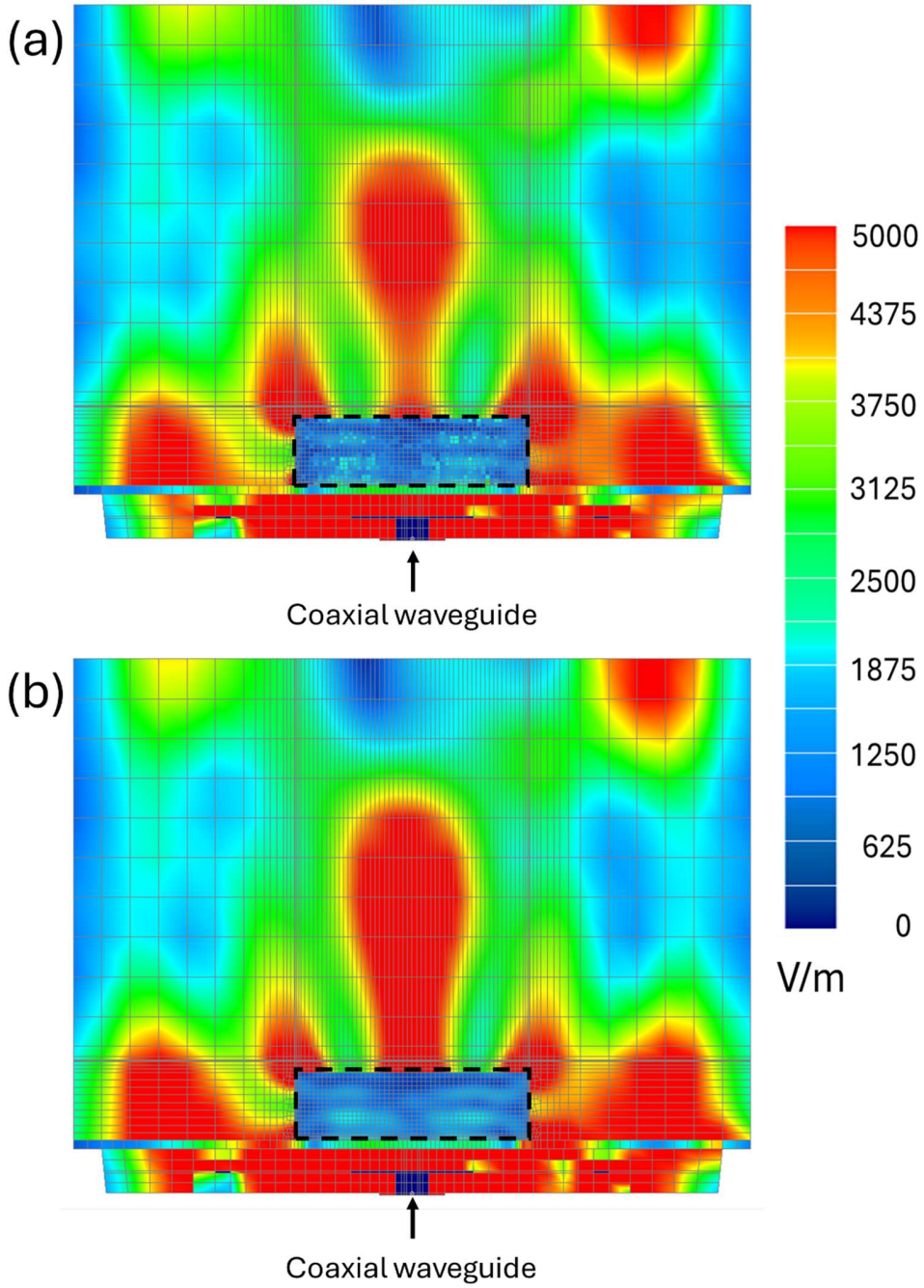

677

678 **Figure 7**. Frontal cross-section of the electric field distribution (V/m) during MW reheating of cooked

679 rice on a flatbed microwave oven (t=20 s) simulated using a two-element (a) and apparent

680 homogeneous (b) model.

681

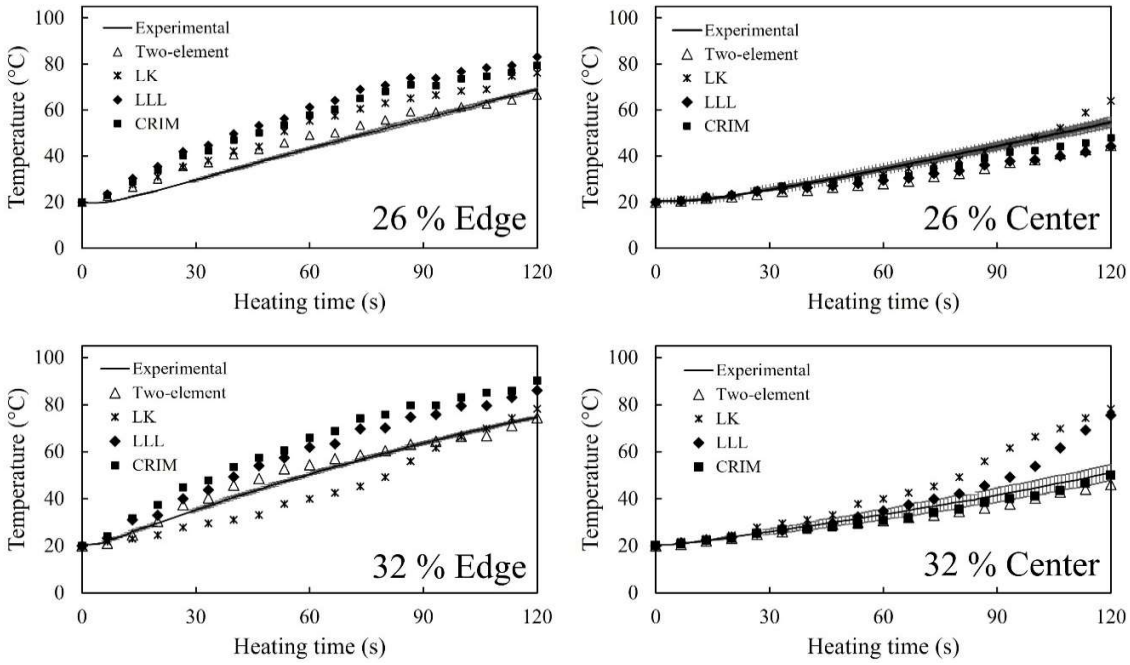

682

683 **Figure 8**. Experimental (mean values ± standard deviation, *n*=3) and simulated temperatures as

684 function of MW heating time for: 26 % porosity rice at the edge (a), 26 % porosity rice at the center

685 (b), 32 % porosity rice at the edge (c), and 32 % porosity rice at the center (d) of the container.

686

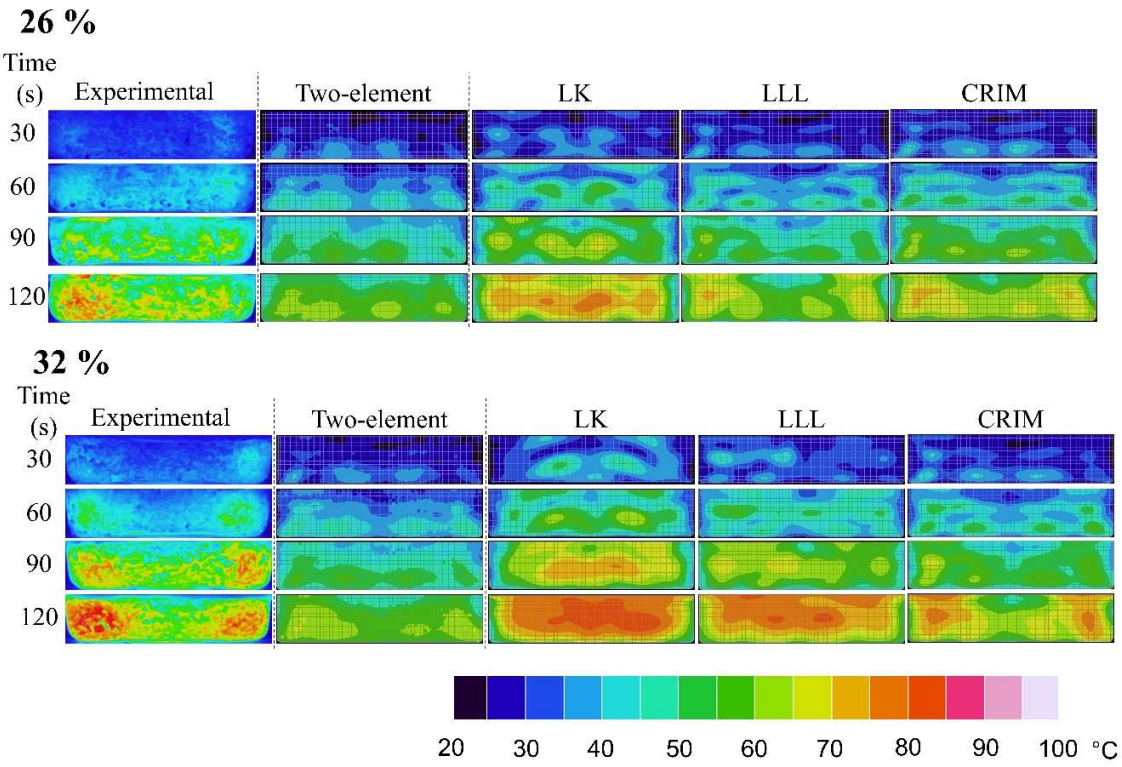

687

688 **Figure 9.** Experimental temperature distribution of the longitudinal cross-section (Z-Y view) of 26 and

689 32 % porosity rice samples during heating on a flatbed MW oven and simulated results using different

690 approaches.

691

Figure S1.a shows the longitudinal cross-section (Z-Y view) of 26 and 32 % porosity rice samples before the heating treatments. The volume remains unchanged between samples. The corresponding amount for each porosity is placed inside the container gradually, while carefully mashing it until reaching the fixed volume. It is worth noting that although there is only a difference of 6 % in porosity, differences can be visually appreciated between the samples.

Figure S1. Longitudinal cross-section (Z-Y view) of 26 (a) and 32 % (b) porosity rice samples before heating on a flatbed microwave oven.

Figure S2.a shows the mesh elements of the different domains in the flatbed microwave model. The equipment was dismantled, and the dimensions of the different components were measured. Figure S2.b illustrates the relation between the mesh of the stationary and rotating domains at the bottom of the cavity.

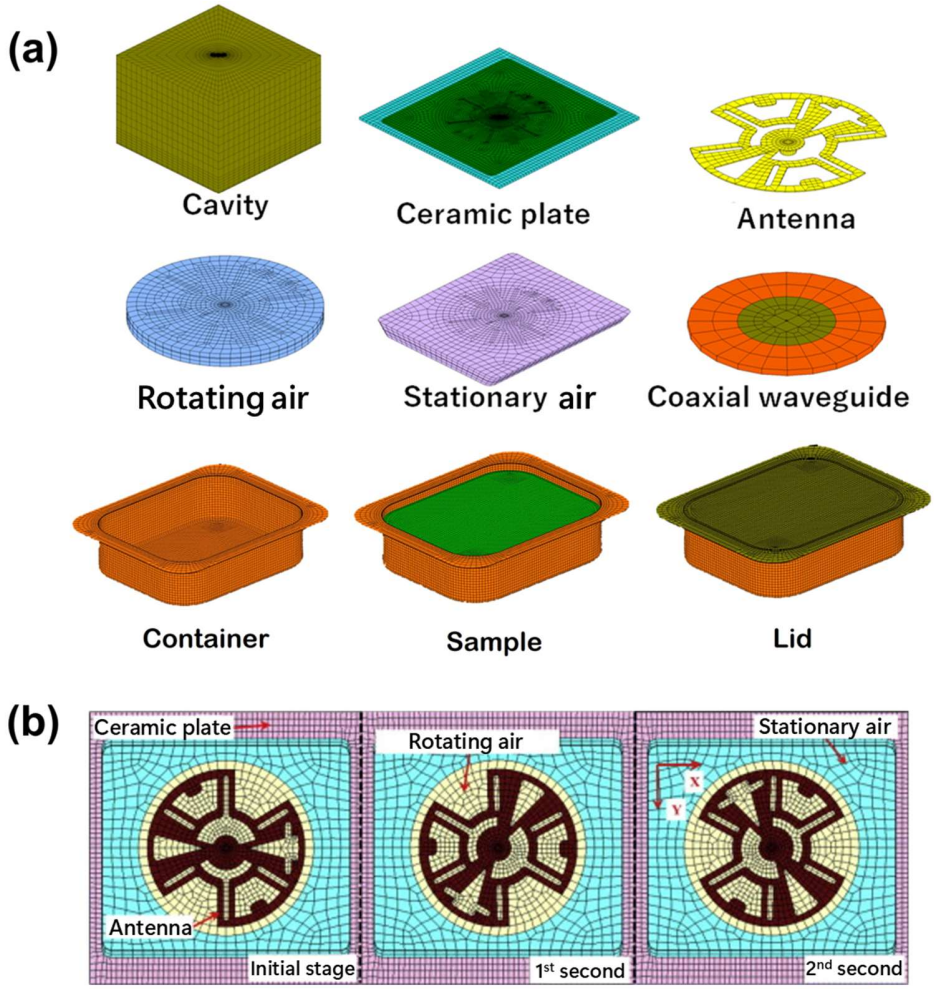

Figure S2. Mesh of each domain in the 3D model of the flatbed microwave oven used in this study (a) and view direction of the stationary and rotating domains at the bottom of the cavity from the X-Y (b).